Article

Triterpenoids from Kochiae Fructus: Glucose Uptake in 3T3-L1 Adipocytes and α-Glucosidase Inhibition, In Silico Molecular Docking

Xue-Lin Chen [1,2,†], Kun Zhang [1,2,†], Xia Zhao [1], Han-Lei Wang [1,2], Mei Han [1,2], Ru Li [1,2], Zhen-Nan Zhang [1,2] and Yu-Mei Zhang [1,2,*]

[1] Key Laboratory of Tropical Plant Resource and Sustainable Use, Xishuangbanna Tropical Botanical Garden, Chinese Academy of Sciences, Kunming 650223, China
[2] School of Life Science, University of Chinese Academy of Sciences, Beijing 100049, China
*   Correspondence: zymei@xtbg.ac.cn; Tel.: +86-871-6511-2766
†   These authors contributed equally to this work.

Abstract: In this study, three new triterpenes (**1–3**) and fourteen known triterpenoids (**4–17**) were isolated from the ethanol extract of Kochiae Fructus, and their structures were elucidated by analyzing UV, IR, HR-ESI-MS, 1D, and 2D NMR spectroscopic data. Among them, compounds **6**, **8**, and **11−17** were isolated for the first time from this plant. The screening results of the glucose uptake experiment indicated that compound **13** had a potent effect on glucose uptake in 3T3-L1 adipocytes at 20 μM. Meanwhile, compounds **3**, **9** and **13** exhibited significant inhibitory activities against α-glucosidase, with IC_{50} values of 23.50 ± 3.37, 4.29 ± 0.52, and 16.99 ± 2.70 μM, respectively, and their α-glucosidase inhibitory activities were reported for the first time. According to the enzyme kinetics using Lineweaver–Burk and Dixon plots, we found that compounds **3**, **9** and **13** were α-glucosidase mixed-type inhibitors with K_i values of 56.86 ± 1.23, 48.88 ± 0.07 and 13.63 ± 0.42 μM, respectively. In silico molecular docking analysis showed that compounds **3** and **13** possessed superior binding capacities with α-glucosidase (3A4A AutoDock score: -4.99 and -4.63 kcal/mol). Whereas compound **9** showed $+2.74$ kcal/mol, which indicated compound **9** exerted the effect of inhibiting α-glucosidase activity by preferentially binding to the enzyme−substrate complex. As a result, compounds **3**, **9** and **13** could have therapeutic potentials for type 2 diabetes mellitus, due to their potent hypoglycemic activities.

Keywords: Kochiae Fructus; *Kochia scoparia*; triterpenoids; α-glucosidase; glucose uptake; molecular docking

1. Introduction

Diabetes mellitus is a chronic metabolic illness that has become a global public health problem [1]. According to the International Diabetes Federation (IDF), approximately 536.6 million adults between the ages of 20 and 79 years had diabetes mellitus in 2021 and this number is expected to rise to 783.2 million by 2045 [2]. Type 2 diabetes mellitus (T2DM) accounts for over 90% of all patients with diabetes and is characterized mainly by insulin resistance, reduction of insulin secretion, and hyperglycemia [3]. It is well established that decreased peripheral glucose uptake, combined with augmented endogenous glucose production, are characteristic features of insulin resistance [4]. Glucosidase enzymes catalyze hydrolysis of starch into simple sugars. In humans, these enzymes aid digestion of dietary carbohydrates and starches to produce glucose for intestinal absorption, which in turn, leads to an increase in blood glucose levels [5]. From these perspectives, enhancing the glucose uptake of organs or tissues [6], as well as inhibiting the activity of α-glucosidase [7], are major strategies for T2DM patients to maintain proper blood glucose levels.

Adipocytes play a vital role in glucose metabolism. 3T3-L1 preadipocytes, after differentiation to adipocytes, serve as excellent in vitro models and are useful tools in understanding the glucose metabolism [8]. Kim SH previously proved that berberine-activated, GLUT1-mediated glucose uptake in 3T3-L1 adipocytes [9]. Recent research by Shyni GL found that chebulagic acid from *Terminalia chebula* enhanced insulin-mediated glucose uptake in 3T3-L1 adipocytes via the PPARγ signaling pathway [10]. This research provided proof that the 3T3-L1 adipocyte glucose uptake model was an effective and feasible way for T2DM research. Furthermore, early studies have shown that the inhibition of α-glucosidase activity could retard the absorption of glucose and decrease the postprandial blood glucose levels [11,12]. Therefore, α-glucosidase has been taken as a key target for treating diabetes, and the inhibitors of α-glucosidase can be developed into effective therapeutic drugs to treat T2DM [13].

Kochiae Fructus (KF) is the dried fruits of *Kochia scoparia*, which is an important Chinese herbal medicine. It contains a variety of bioactive components such as triterpenoids [14,15], flavonoids [16,17], carbohydrates [18], amino acids [18], organic acids [18], and essential oils [19]. KF was listed as 'top grade' medicinal material by the *Shennong's Classic of Materia Medica* and has been used in traditional Chinese medicine to treat rubella, eczema, cutaneous pruritus, and difficulty and pain in micturition [20,21]. Modern pharmacological research showed that KF possessed a broad range of pharmacological activities, including anti-inflammatory [22], hypoglycemic [23], antioxidant [24], anticancer [25], antifungal [26], anti-pruritogenic [27], antinociceptive [28], antiallergic [29], and hepatoprotective [30] activity.

According to literature, the antidiabetic activity of the n-butanol fraction of KF had been investigated, however, there are few reports on the hypoglycemic mechanism of corresponding chemical constituents of KF. Therefore, in this study, chemical constituents of KF were isolated and identified. Furthermore, the glucose uptake assay and α-glucosidase inhibition experiment were used to explore its hypoglycemic effect and the possible hypoglycemic mechanism. In addition, in silico molecular docking study was used to determine the inhibitory activities of candidate compounds against α-glucosidase. Herein are reported the isolation and structure determination of three new triterpenes (**1**−**3**) along with fourteen known triterpenoids (**4**−**17**) from the ethanol extract of KF. Among them, compounds **6**, **8**, and **11**−**17** were isolated for the first time from this plant. In addition, the glucose uptake effect of compound **13** and the inhibitory activities of compounds **3**, **9**, and **13** against α-glucosidase were reported for the first time.

2. Results and Discussion

2.1. Chemistry

Compound **1** was obtained as a white amorphous powder. The molecular formula was established to be $C_{41}H_{62}O_{15}$ (eleven degrees of unsaturation) by HR-ESI-MS at m/z 396.1971 $[M-2H]^{2-}$ (calcd 396.1972), which was confirmed by ^{13}C and DEPT NMR spectra. The ^{13}C NMR spectrum (Table 1) revealed signals due to six methyl carbons at δ_C 33.7 (C-29), 26.4 (C-27), 24.1 (C-30), 17.7 (C-26), 16.4 (C-25) and 12.2 (C-24); one oxygen-bearing methine carbon at δ_C 86.6; a pair of olefinic carbons at δ_C 123.6 (C-12) and 145.3 (C-13); and two carboxylic acid carbons at δ_C 181.9 (C-28) and 181.5 (C-23). These data, coupled with corresponding information from the ^1H NMR spectrum [six methyl groups as singlets at δ_H 0.80 (H-26), 0.90 (H-29), 0.93 (H-30), 0.96 (H-25), 1.14 (H-24) and 1.16 (H-27); hydroxymethine proton at δ_H 4.05 (dd, J = 11.5, 4.0 Hz, H-3); a proton attributed to H-18 at δ_H 2.84 (dd, J = 13.5, 4.0 Hz); and a triplet vinyl proton at δ_H 5.23 (1H, brs, H-12)] (Table 2) and 2D NMR spectra, confirmed that compound **1** had an oleanolic acid skeleton. In the HMBC spectrum, correlation signals from δ_H 4.05 (H-3) to δ_C 26.6 (C-2), 54.0 (C-4), 181.5 (C-23), and 12.2 (C-24) were exhibited, which confirmed the location of the hydroxyl group at C-3. In the ROESY contour map, correlations between H-3 and H-5 were detected, which confirmed that H-3 was α-oriented. The aforementioned NMR data of compound **1** were closely similar to those of momordin Ic [31], except for the signals from ring A, a carboxyl group at C-23 position.
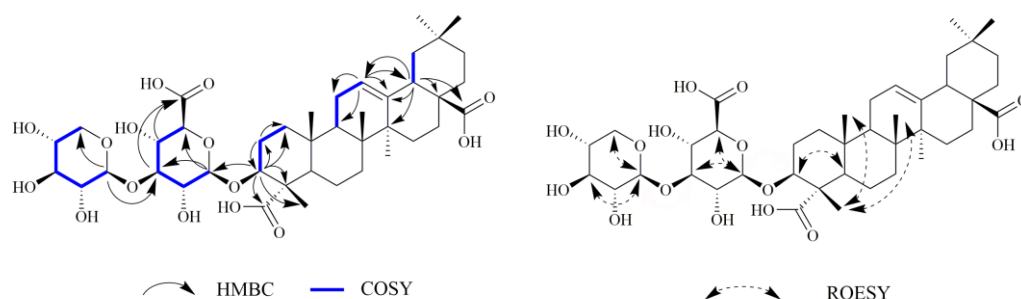
In the HMBC spectrum, correlation signals from δ_H 1.14 (H-24) to δ_C 86.6 (C-3) and 181.5 (C-23) were exhibited, which confirmed the location of the carboxyl group at C-23 (Figure 1). Furthermore, the hypothesis was supported by the correlations between H-25 (δ_H 0.96), H-24 (δ_H 1.14), and H-26 (δ_H 0.80) in the ROESY contour map (Figure 1). From the above data, the structure of compound **1** was deduced to be 3(β)-3-*O*-β-D-xylopyranosly(1→3) -β-D-glucopyranosiduronic acid-12-en-23,28-dioic acid.

Table 1. ^{1}H NMR (500 MHz) and ^{13}C NMR (125 MHz) data of compounds **1–3** in methanol-d_4.

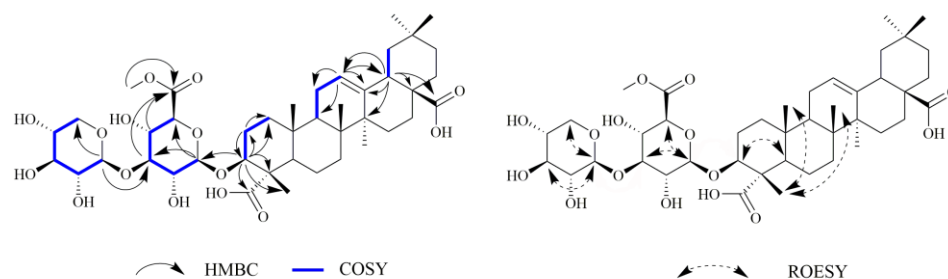| No.	1 δ_H, (J in Hz)	δ_C	2 δ_H, (J in Hz)	δ_C	3 δ_H, (J in Hz)	δ_C
1	1.67, overlapped	39.7	1.66, overlapped	39.7	1.92, m	48.3
	1.08, overlapped		1.08, overlapped		0.88, m	
2	1.87, m	26.6	1.83, m	26.6	3.62, m	69.6
	1.68, m		1.67, m			
3	4.05, dd (11.5, 4.0)	86.6	4.05, dd (11.5, 4.5)	86.6	2.90, d (9.5)	84.6
4		54.0		54.1		40.7
5	1.49, m	53.1	1.49, m	53.1	0.84, m	56.9
6	2.00, td (13.5, 3.5)	24.2	2.01, td (13.5, 4.0)	24.2	2.04, td (13.5, 3.5)	24.1
	1.59, m		1.60, m		1.70, m	
7	1.53, overlapped	33.7	1.53, overlapped	33.7	1.56, overlapped	34.0
	1.53, overlapped		1.53, overlapped		1.56, overlapped	
8		41.0		41.0		40.9
9	1.65, overlapped	49.1	1.64, overlapped	49.1	1.62, overlapped	49.2
10		37.6		37.6		39.4
11	1.92, m	24.6	1.93, m	24.6	1.92, m	24.8
	1.90, m		1.91, m		1.90, m	
12	5.23, brs	123.6	5.24, brs	123.6	5.27, brs	123.8
13		145.3		145.6		145.2
14		43.0		43.1		43.1
15	1.76, overlapped	29.0	1.76, overlapped	29.0	1.79, overlapped	29.0
	1.05, overlapped		1.05, overlapped		1.05, overlapped	
16	1.57, overlapped	21.9	1.57, overlapped	21.9	1.52, overlapped	19.7
	1.57, overlapped		1.57, overlapped		1.52, overlapped	
17		47.8		47.8		48.2
18	2.84, dd (13.5, 4.0)	42.9	2.85, dd (14.0, 4.0)	42.9	2.86, dd (14.0, 4.0)	42.7
19	1.71, m	47.4	1.69, m	47.4	1.70, m	47.4
	1.11, m		1.11, m		1.13, m	
20		31.8		31.8		31.7
21	1.38, td (13.5, 3.5)	35.0	1.39, td (13.5, 4.0)	35.0	1.39, m	35.0
	1.21, m		1.22, m		1.21, m	
22	1.73, overlapped	33.9	1.72, overlapped	34.0	1.72, overlapped	33.3
	1.27, overlapped		1.27, overlapped		1.32, overlapped	
23		181.5		181.7	1.01, s	29.4
24	1.14, s	12.2	1.14, s	12.4	0.80, s	17.9
25	0.96, s	16.4	0.96, s	16.4	1.01, s	17.3
26	0.80, s	17.7	0.81, s	17.7	0.80, s	17.6
27	1.16, s	26.4	1.17, s	26.5	1.16, s	26.5
28		181.9		182.0		178.2
29	0.90, s	33.7	0.91, s	33.7	0.91, s	33.6
30	0.93, s	24.1	0.94, s	24.1	0.94, s	24.1

Table 2. ^{1}H NMR (500 MHz) and ^{13}C NMR (125 MHz) data of the sugar moieties for compounds **1–3** in methanol-d_4.

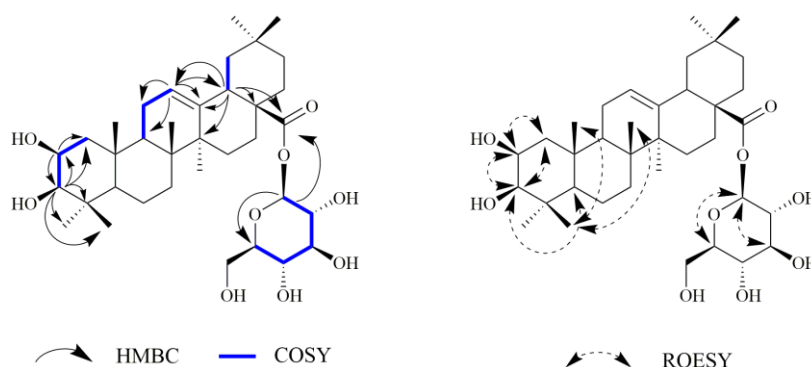| No.	1 δ_H, (J in Hz)	δ_C	2 δ_H, (J in Hz)	δ_C	3 δ_H, (J in Hz)	δ_C
GlcA-at-C-3					Glc-at-C-28	
1′	4.37, d (7.5)	105.5	4.39, d (7.5)	105.5	5.38, d (8.0)	95.9
2′	3.35, d (7.5)	74.6	3.34, d (7.5)	74.6	3.31, m	74.1
3′	3.50, m	86.3	3.52, m	86.1	3.40, m	78.5
4′	3.56, m	71.8	3.57, m	71.7	3.34, m	71.3
5′	3.76, m	76.4	3.83, d (9.5)	76.5	3.34, m	78.9
6′		171.4		171.2	3.81, dd (12.0, 1.5)	62.6
					3.68, dt (12.0, 2.0)	
6′-OMe			3.77, s	53.0		
Xyl→glc-C-3						
1″	4.50, d (7.5)	105.9	4.52, d (7.5)	105.9		
2″	3.24, m	75.4	3.24, m	75.4		
3″	3.32, m	77.7	3.32, m	77.7		
4″	3.47, m	71.2	3.49, m	71.2		
5″	3.89, dd (11.5, 5.5)	67.2	3.89, dd (11.5, 5.5)	67.2		
	3.20, dd (11.5, 5.5)		3.20, dd (11.5, 5.5)			

Figure 1. Key HMBC, COSY, and ROESY correlations of compound **1**.

Compound **2** was obtained as a white amorphous powder. Its molecular formula was determined to be $C_{42}H_{64}O_{15}$, on the basis of a negative HR-ESI-MS profile (*m/z*: 403.2053 [M-2H]$^{2-}$, calcd 403.2050), implying eleven degrees of unsaturation. The ^{13}C NMR (Table 1) and HSQC spectra of compound **2** showed 42 carbon signals comprising ten quaternary carbon atoms [including two carboxylic acid carbon at δ_C 182.0 (C-28) and 181.7 (C-23)]; fourteen methine carbons [including an olefinic carbon at δ_C 123.6 (C-12)]; one oxymethine carbon at δ_C 86.6 (C-3); and two anomeric carbon signals at δ_C 105.5 (C-glcA-1) and 105.9 (C-xyl-1)]; eleven methylenes; six methyls; and a methoxy carbon (δ_C 53.0). The ^{1}H NMR spectrum of compound **2** (Table 1) exhibited six methyl groups as singlets at δ_H 0.81 (H-26), 0.91 (H-29), 0.94 (H-30), 0.96 (H-25), 1.14 (H-24) and 1.17 (H-27); hydroxymethine proton at δ_H 4.05 (dd, *J* = 11.5, 4.5 Hz, H-3); a proton attributed to H-18 at δ_H 2.85 (dd, *J* = 14.0, 4.0 Hz); a triplet vinyl proton at δ_H 5.24 (1H, brs, H-12); and a methoxy group at δ_H 3.77 (3H, s). Comparison of ^{1}H and ^{13}C NMR values and the analysis of the HMBC correlations showed that compound **2** was entirely consistent with compound **1,** except for one methoxy carbon (δ_C 53.0, δ_H 3.77) that occurred in compound **2**. In the HMBC spectrum, correlation signals from δ_H 3.77 to δ_C 171.2 (C-glc-6) were exhibited, which confirmed the location of the methoxy group at C-6′ of the glucuronopyranose unit (Figure 2). According to the above data, the structure of compound **2** was elucidated as 3(β)-3-*O*-β-D-xylopyranosly(1→3) -β-D-glucopyranosiduronic acid 6-methyl ester-12-en-23,28-dioic acid.
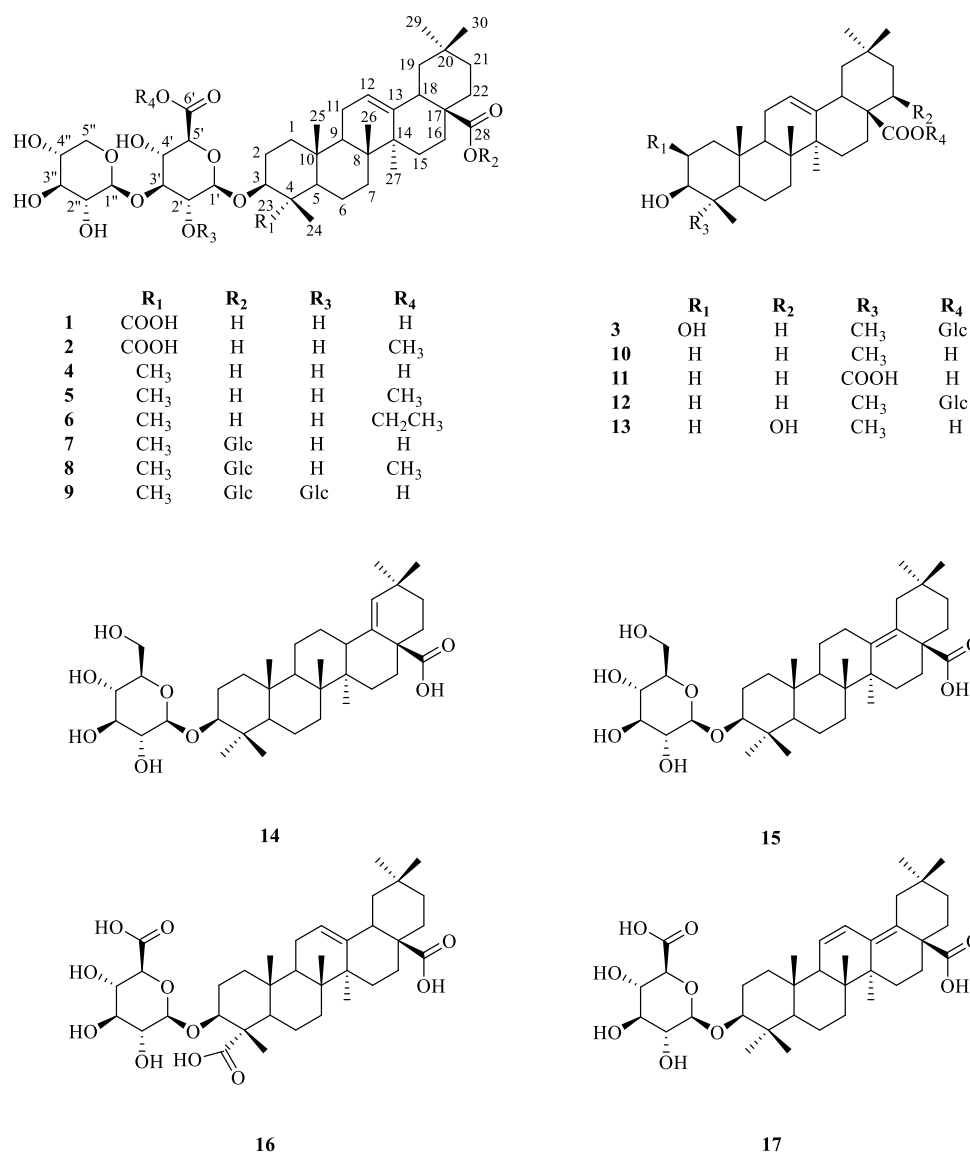
Figure 2. Key HMBC, COSY, and ROESY correlations of compound **2**.

Compound **3** was obtained as a white powder with a molecular formula of $C_{36}H_{58}O_9$ (eight degrees of unsaturation), as determined by the pseudo-molecular ion peak at m/z: 657.3973 [M+Na]$^+$ (calcd 657.3973) shown in the HR-ESI-MS spectra. The ^{1}H NMR spectrum of compound **3** (Table 1) revealed seven angular methyl signals at δ_H 0.80 (H-26), 0.80 (H-24), 0.91 (H-29), 0.94 (H-30), 1.01 (H-25), 1.01 (H-23) and 1.16 (H-27); one olefinic proton signal at δ_H 5.27 (1H, brs, H-12); two oxygen-substituted proton signals [δ_H 3.62 (1H, m, H-2) and 2.90 (d, *J* = 9.5 Hz, H-3)]; and a proton attributed to H-18 at δ_H 2.86 (dd, *J* = 14.0, 4.0 Hz). The ^{13}C NMR (Table 1) and HSQC spectra (Figure 3) of compound **3** showed 36 carbon signals including a carboxylic acid carbon [δ_C 178.2 (C-28)]; a pair of olefinic carbons [δ_C 145.2 (C-13) and 123.8 (C-12)]; two oxygenated methine carbons [δ_C 84.6 (C-3) and 69.6 (C-2)]; one anomeric carbon [δ_C 95.9 (C-glc-1)]; and seven methyl carbons [δ_C 33.6 (C-29), 29.4 (C-23), 26.5 (C-27), 24.1 (C-30), 17.9 (C-24), 17.6 (C-26) and 17.3 (C-25)], which were characteristic of the 12-ene triterpene containing two hydroxy groups. The observed HMBC correlations from C-2 (δ_C 69.6) to H-1 (δ_H 1.92 and 0.88), H-3 (δ_H 2.90), and H-23 (δ_H 1.01), and from H-3 (δ_H 2.90) to C-1 (δ_C 48.3), C-2 (δ_C 69.6), C-4 (δ_C 40.7), C-23 (δ_C 29.4), and C-24 (δ_C 17.9), combined with the ^{1}H-^{1}H COSY correlations of H-1/H-2/H-3, established the existence of the two hydroxy groups at C-2 and C-3, respectively. The aforementioned NMR data of compound **3** were closely similar to those of oleanolic acid 28-*O*-β-D-glucopyranosyl ester [32], except for the configuration of the hydroxy group at C-2. In the ROESY spectrum of compound **3** (Figure 3), cross-peaks were observed between H-2/H-3, H-23; H-3/H-2, H-5, H-23, implied that the configurations of hydroxy groups at C-2 and C-3 were both defined as β-orientation. Therefore, the structure of compound **3** was assigned as 2β,3β- Dihydroxyolean-12-en-28-oic acid 28-*O*-β-D-glucopyranoside.

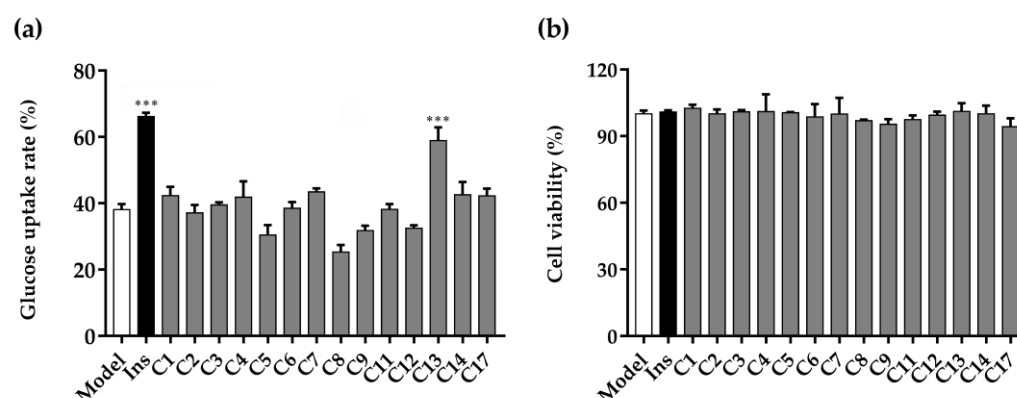**Figure 3.** Key HMBC, COSY, and ROESY correlations of compound **3**.

The other fourteen known compounds (Figure 4) were characterized as momordin Ic (**4**) [31], momordin Ic 6′-methyl ester (**5**) [33], momordin Ic ethyl ester (**6**) [34], momordin IIc (**7**) [35], momordin IIc 6′-methyl ester (**8**) [14], 2′-*O*-β-D-glucopyranosyl momordin IIc (**9**) [33], oleanolic acid (**10**) [36], gypsogenic acid (**11**) [37], oleanolic acid 28-*O*-β-D-glucopyranosyl ester (**12**) [32], 3β,22β-butyryloxy-olean-12-en-28-oic acid (**13**) [38], (3β)-3-(β-D-glucopyranosyloxy)olean-18-en-28-oic acid (**14**) [39], (3β)-3-(β-D-glucopyranosyloxy)olean-13(18)-en-28-oic acid (**15**) [40], (3β)-3-(β-D-glucuronopyranosyloxy)olean-12-en-23,28-dioic acid (**16**) [41], (3β)-3-(β-D-glucuronopyranosyloxy)olean-11,13-dien-28-oic acid (**17**) [42].

	R_1	R_2	R_3	R_4
1	COOH	H	H	H
2	COOH	H	H	CH_3
4	CH_3	H	H	H
5	CH_3	H	H	CH_3
6	CH_3	H	H	CH_2CH_3
7	CH_3	Glc	H	H
8	CH_3	Glc	H	CH_3
9	CH_3	Glc	Glc	H

	R_1	R_2	R_3	R_4
3	OH	H	CH_3	Glc
10	H	H	CH_3	H
11	H	H	COOH	H
12	H	H	CH_3	Glc
13	H	OH	CH_3	H

14

15

16

17

Figure 4. Chemical structures of compounds **1**−**17** isolated from Kochiae Fructus.

2.2. Glucose Uptake and Cell Viability

Using 3T3-L1 adipose model cells, the insulin-induced glucose uptake-enhancing assay was performed to determine glucose consumption after treatment with the compounds. The activity represents the compounds' potential to reduce insulin resistance in body tissues, such as adipocytes, resulting in hypoglycemic effects [43]. To examine the effects of the isolated compounds from KF with glucose uptake in 3T3-L1 adipocytes, 14 compounds (purity $\geq$ 95%; HPLC) were screened for their abilities to enhance glucose uptake upon the induction of insulin against fully differentiated 3T3-L1 cells. As shown in Figure 5a, the insulin group could significantly promote the glucose uptake rates of 3T3-L1 adipocytes compared to the control group with a significant difference ($p < 0.001$). Simultaneously, compound **13** had a strong effect on glucose uptake in 3T3-L1 adipocytes at 20 µM ($p < 0.001$). Additionally, the results of cell viability showed that compared to the control group, the isolated compounds had no cytotoxicity (Figure 5b). In conclusion, compound **13** had a significant capability to promote glucose uptake in 3T3-L1 adipocytes, and without inhibitory effects on cell viability.

(a) **(b)**

Figure 5. Glucose uptake and cell viability in 3T3-L1 adipocytes. (**a**) Glucose uptake rate of compounds **1**−**9**, **11**−**14**, and **17**. (**b**) Cell viability of compounds **1**−**9**, **11**−**14**, and **17**. Ins, insulin (positive control); C, compound; compounds at 20 μM and insulin at 250 ng/mL; all values are mean ± SD from a least three independent experiments, and each group is compared with model group, significance is denoted by symbols: *** $p < 0.001$.
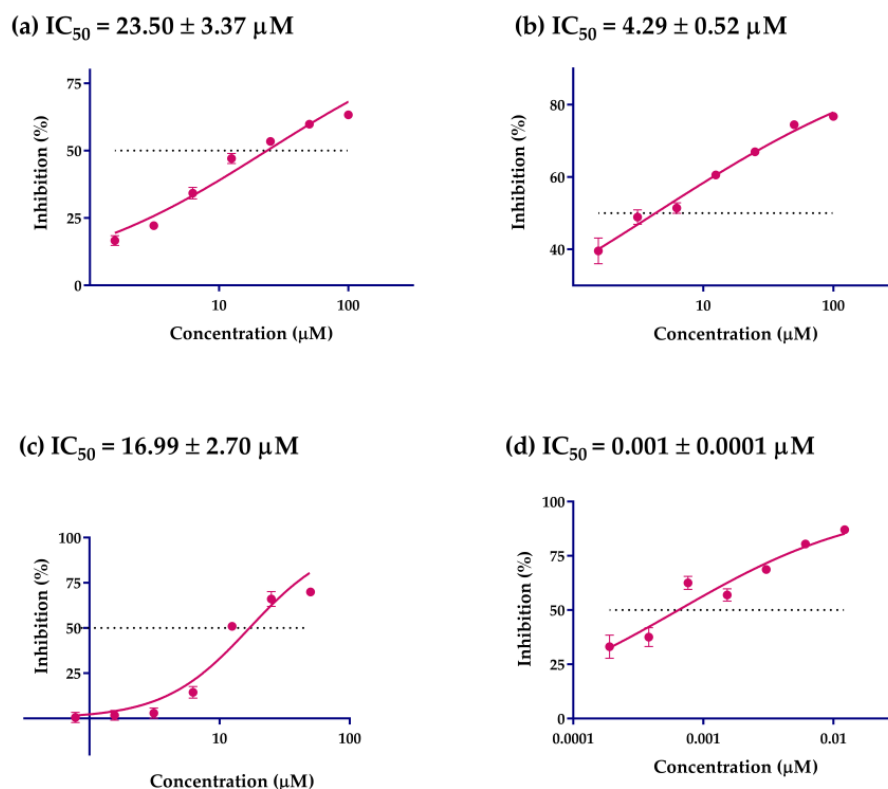
2.3. α-Glucosidase Inhibition Activity

α-Glucosidase inhibitors exert hypoglycemic effects by slowing the digestion of carbohydrates and delaying glucose absorption [44]. Identification of potential α-glucosidase inhibitors were done by in vitro screening of 14 pentacyclic triterpenes (purity ≥ 95%; HPLC) using an α-glucosidase inhibition experiment. The results are shown in Table 3. Compounds **1**–**9**, **11**–**14**, and **17** exhibited varying degrees of α-glucosidase inhibitory activity, with inhibitory rates between 13.71 ± 0.54 and 74.41 ± 1.02%. Further tests of α-glucosidase inhibitory activities on compounds **3**, **9**, and **13** were carried out, and the results are shown in Figure 6. Compounds **3**, **9**, and **13** showed the most potent α-glucosidase inhibition activities ($p < 0.05$) with an IC_{50} value of 23.50 ± 3.37, 4.29 ± 0.52, and 16.99 ± 2.70 μM, respectively. This was the first report of the α-glucosidase inhibitory activities of compounds **3**, **9**, and **13**. Our study showed that compounds **3** and **13** have two hydroxyl groups over the ring of the pentacyclic triterpenes, which indicated the hydroxyl group in the ring of the pentacyclic triterpenes may be an effective functional group as potent α-glucosidase inhibitors. Previous studies also reported that the hydroxyl group of pentacyclic triterpenes has been found to confer a variety of biological properties, such as anti-tumor, anti-inflammatory, antimicrobial and hypoglycemic activities [45].

Table 3. α-Glucosidase inhibitory activities of compounds **1**−**9**, **11**−**14**, and **17**.

Compounds	Inhibitory Rate (%)	IC$_{50}$ (μM)
Acarbose [A]	87.04 ± 0.29 [a]	0.001 ± 0.00
1 [B]	13.71 ± 0.54 [j]	>50
2 [B]	14.05 ± 4.90 [j]	>50
3 [B]	59.79 ± 1.04 [d]	23.50 ± 3.37
4 [B]	26.28 ± 1.01 [i]	>50
5 [B]	29.62 ± 2.26 [i]	>50
6 [B]	35.00 ± 0.40 [h]	>50
7 [B]	52.71 ± 0.85 [f]	>50
8 [B]	57.02 ± 36.3 [e]	>50
9 [B]	74.41 ± 1.02 [b]	4.29 ± 0.52
11 [B]	53.98 ± 1.65 [e]	>50
12 [B]	41.48 ± 1.66 [g]	>50
13 [B]	69.91 ± 0.59 [c]	16.99 ± 2.70
14 [B]	17.49 ± 4.45 [j]	>50
17 [B]	55.68 ± 0.17 [e]	>50

Data were expressed as the mean value ± SD ($n = 3$); means followed by the different letters ([a−j]) are significantly different ($p < 0.05$); [A], percent inhibition at a concentration of 0.012 μM; [B], percent inhibition at a concentration of 50 μM.

(a) IC$_{50}$ = 23.50 ± 3.37 μM

(b) IC$_{50}$ = 4.29 ± 0.52 μM

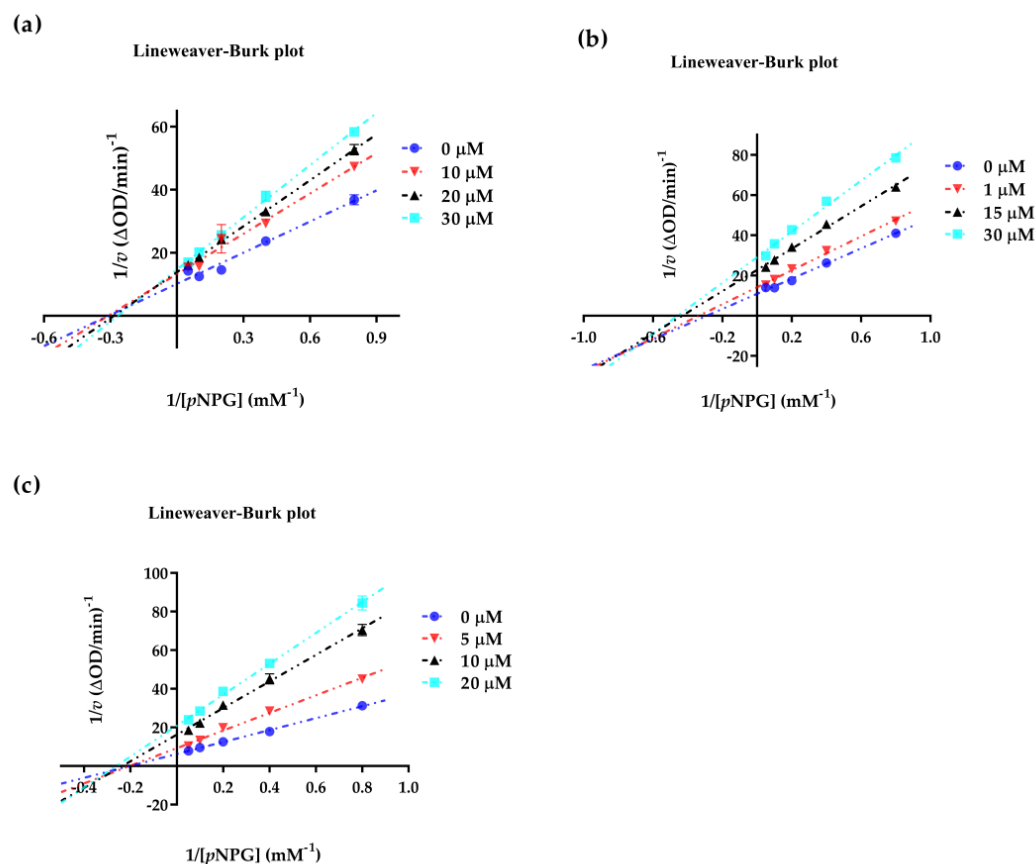**(c)** IC$_{50}$ = 16.99 ± 2.70 μM

(d) IC$_{50}$ = 0.001 ± 0.0001 μM

Figure 6. *α*-Glucosidase inhibitory effects of compounds **3**, **9**, and **13**. (**a**) Log concentration–inhibition rate fitting curve of compound **3**. (**b**) Log concentration–inhibition rate fitting curve of compound **9**. (**c**) Log concentration–inhibition rate fitting curve of compound **13**. (**d**) Log concentration–inhibition rate fitting curve of acarbose. Calculated IC$_{50}$ values of different groups by Statistical Product and Service Solutions (SPSS, version: 21.0), and all values are mean ± SD from a least three independent experiments.

2.4. Enzyme Kinetic Equation

It is well accepted that enzyme kinetics can provided some useful information for predicting the interactions between the ligands and enzymes. To clarify how and where triterpenes bind to *α*-glucosidase, we first measured the enzyme kinetics of compounds **3**, **9** and **13,** by using methods similar to those described in the literature [46]. As shown in Figure 7, the concentrations of $1/[p\text{NPG}]$ are displayed on the *X*-axis, and $1/v$ values obtained from the Lineweaver–Burk plot are shown along the *Y*-axis. The plots of compound **3** intersected in the second quadrant, meaning that the Vmax values decreased and the Km values increased with the increased concentration of inhibitors (Figure 7a). The plots of compounds **9** and **13** intersected in the third quadrant, meaning that both the Km and Vmax values decreased with the increased concentration of inhibitors (Figure 7b,c). The results indicated that compounds **3**, **9** and **13** caused a mixed-type inhibition, which meant they could bind to both the free enzyme and the enzyme-substrate complex [47].

We also examined Dixon plots of how compounds **3**, **9** and **13** affect *α*-glucosidase. As shown in Figure 8, these plots further confirmed that compounds **3**, **9** and **13** are mixed-type *α*-glucosidase inhibitors. The K_i values of compounds **3**, **9** and *13* were 56.86 ± 1.23, 48.88 ± 0.07 and 13.63 ± 0.42 μM, respectively, while the K_i' values of these compounds were 47.89 ± 1.37, 19.52 ± 0.26 and 8.82 ± 0.06 μM, respectively. K_i is the equilibrium constant for the inhibitor binding to *α*-glucosidase, and K_i' is the equilibrium constant for the inhibitor binding to the *α*-glucosidase−*p*NPG complex [48]. The results showed that the K_i' values were smaller than the K_i values, which indicated that the inhibitor−enzyme−substrate complex binding affinity exceeds the binding affinity of the inhibitor−enzyme. The binding sites and mechanism underlying inhibition have yet to be determined. However, the results of compounds **3**, **9** and **13** bound to either *α*-glucosidase,

or the α-glucosidase$-p$NPG complex, further confirmed that compounds **3**, **9** and **13** are mixed$-$competitive inhibition against α-glucosidase.
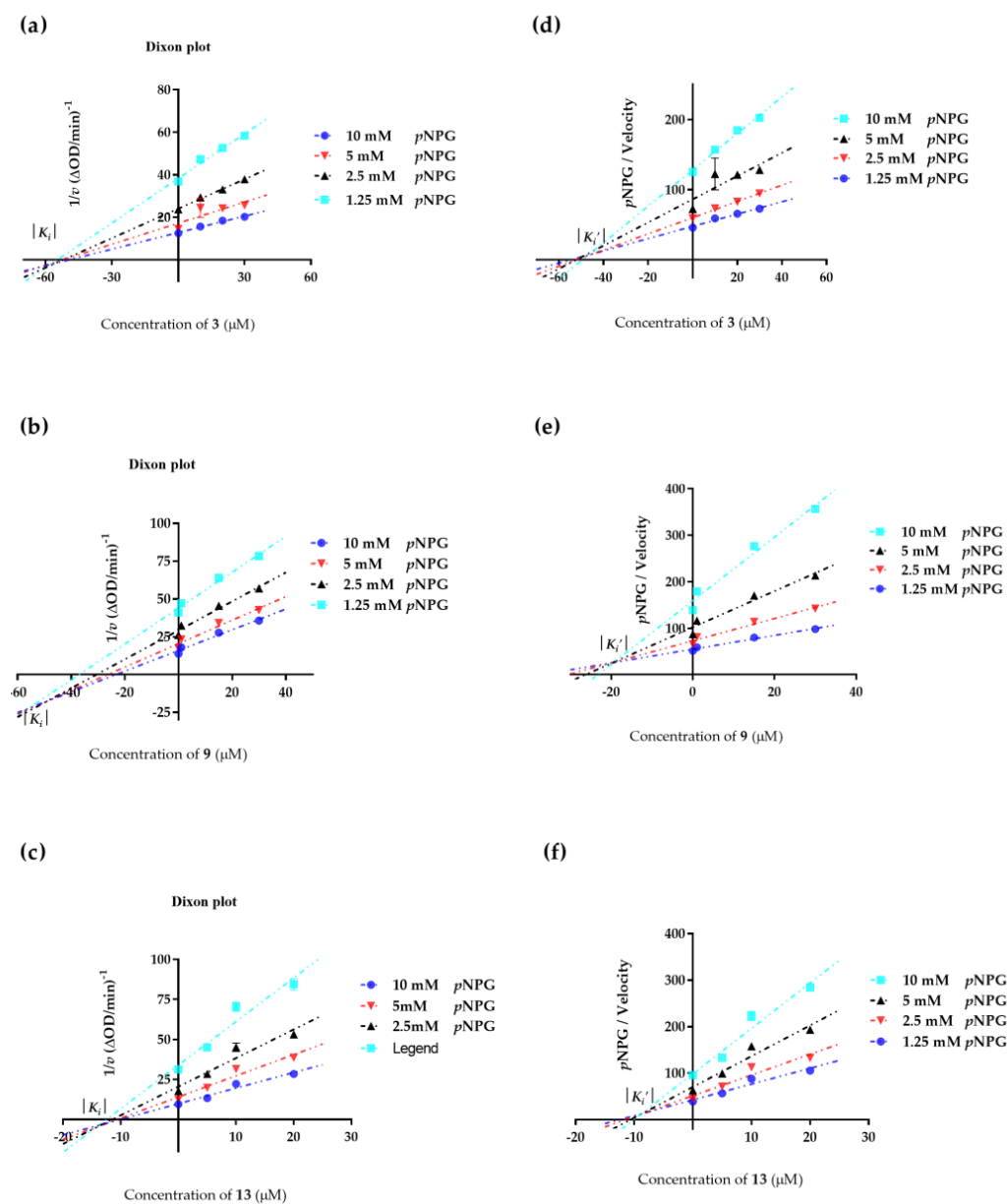
(a)

(b)

(c)

Figure 7. The Lineweaver–Burk plot for α-glucosidase inhibition of compounds **3**, **9**, and **13**. (**a**) $1/[p$NPG$]-1/v$ fitting curve of compound **3**. (**b**) $1/[p$NPG$]-1/v$ fitting curve of compound **9**. (**c**) $1/[p$NPG$]-1/v$ fitting curve of compound **13**. All values are mean $\pm$ SD from at least three independent experiments.
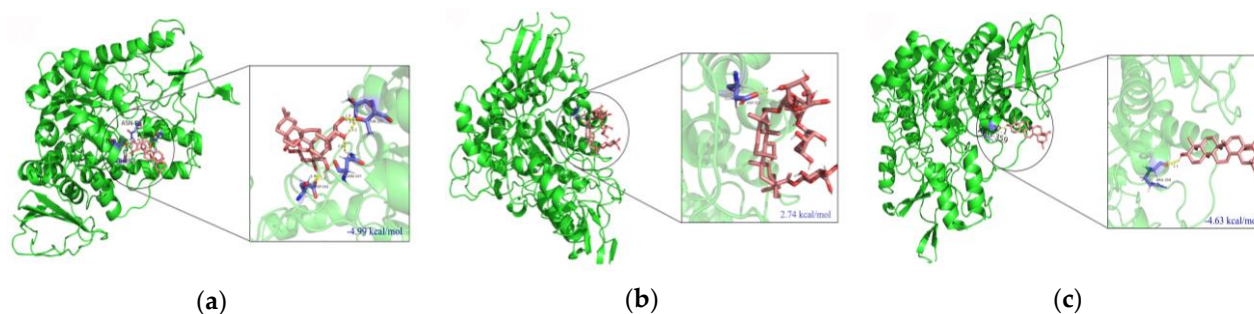
2.5. Molecular Docking

Molecular docking is a key tool in structural molecular biology and computer-assisted drug design. The goal of ligand–protein docking is to predict the predominant binding modes of a ligand with a protein of known 3D structure [49]. The calculated binding energies of 2β,3β-dihydroxyolean-12-en-28-oic acid 28-O-β-D-glucopyranoside (**3**), and 22β-hydroxy-oleanolic acid (**13**) with α-glucosidase, were found to be -4.99 and -4.63 kcal/mol, respectively. But the binding energy of compound **9** with α-glucosidase was found to be $+2.74$ kcal/mol, which indicated poor binding (Figure 9). This result further suggested that compound **9** exerted the effect of inhibiting α-glucosidase activity by preferentially binding to the enzyme–substrate complex. This coincided with the results of the enzyme kinetic analysis, in which the K_i and K_i' values of compound **9** were 48.88 ± 0.07 and 19.52 ± 0.26 μM, respectively. Interestingly, significant H-bonding interactions with the hydroxyl groups of compounds **3** and **13** were found in all these binding sites. For compound **3**, there are four residues (Asn 247, Thr 285, Ser 282 and Asp 242) which formed six hydrogen bonds with the compound. Among these, the hydrogen of the hydroxyl groups at the C-2 and C-3 position on the ring A of compound **3** formed four hydrogen-bonding interactions with Asn 247, Thr 285, Ser 282 residues of the enzyme (Figure 10). For compound **13**, only one hydrogen bond was formed between the compound and the residues of α-glucosidase. It was established between the hydrogen of the hydroxyl group at the C-3 position on the ring A of compound **13** and Arg 359, with a
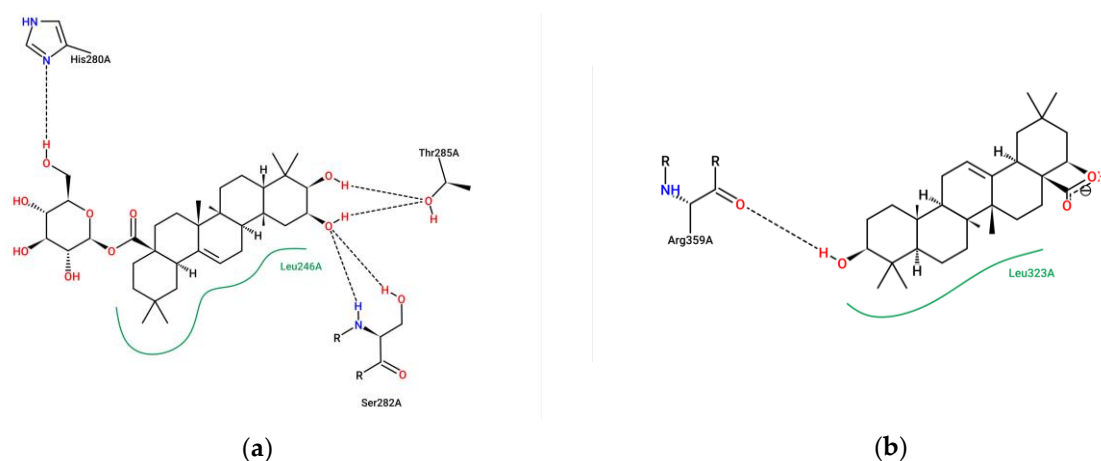
distance of 2.1 Å (Figure 10). This accounts well for the previous observation that hydroxyl groups were essential to improve the inhibitory activity of the compound.

Figure 8. Determination of K_i and K_i' of compounds **3**, **9**, and **13** on α-glucosidase. (**a**) $1/v-$[I] fitting curve of compound **3**. (**b**) $1/v-$[I] fitting curve of compound **9**. (**c**) $1/v-$[I] fitting curve of compound **13**. (**d**) [pNPG]$/v-$[I] fitting curve of compound **3**. (**e**) [pNPG]$/v-$[I] fitting curve of compound **9**. (**f**) [pNPG]$/v-$[I] fitting curve of compound **13**. All values are mean $\pm$ SD from at least three independent experiments.

(**a**)　　　　　　　　　　　　(**b**)　　　　　　　　　　　　(**c**)

Figure 9. Molecular docking pictures of compounds **3**, **9**, and **13** on α-glucosidase of 3A4A. (**a**) 3D-structural model of α-glucosidase bound to compound **3** and the close-up view of the compound **3** molecule bound at the active site of α-glucosidase. (**b**) 3D-structural model of α-glucosidase bound to compound **9** and the close-up view of the compound **9** molecule bound at the active site of α-glucosidase. (**c**) 3D-structural model of α-glucosidase bound to compound **13** and the close-up view of the compound **13** molecule bound at the active site of α-glucosidase. The 3D-structural model of α-glucosidase is shown in green; residues that may be involved in the interactions of compound-binding are drawn with a stick model and shown in purple. The possible hydrogen-bond interactions are indicated with dashed lines (yellow).

(**a**)　　　　　　　　　　　　　　　　　　　　(**b**)

Figure 10. The 2D interaction diagram of the docking poses of compounds **3** (**a**) and **13** (**b**) on α-glucosidase of 3A4A.

3. Materials and Methods

3.1. Chemicals, Reagents and Cell

^{1}H and ^{13}C and 2D NMR spectra were obtained on a Bruker–Avance III-500 MHz (Bruker Corporation, Madison, WI, USA) spectrometer with chemical shifts recorded in δ (ppm), using tetramethylsilane (TMS) as the internal standard, while the coupling constants (*J*) were given in hertz. Mass spectra were obtained on an MS Waters AutoSpec Premier P776 mass spectrometer (ESI-MS) and a UPLC-IT-TOF-MS (HR-ESI-MS), respectively. An IR spectrum was recorded on a BRUKER VERTEX 70 (Bruker Corporation, Madison, WI, USA) spectrometer in KBr pellets. The UV spectrum was measured on a SHIMADZU UV-2401PC (Shimadzu Corporation, Berlin, Germany) series spectrophotometer, with methanol as a solvent. CD spectra was obtained on an Applied Photophysics Chirascan Circular Dichroism Spectrometer (Applied Photophysics Ltd, UK). Optical rotation was taken on an Autopol VI, Serial #91058. Column chromatography was run on silica gel (80–100 mesh and 200–300 mesh) (Qingdao Marine Chemical Co., Ltd., Qingdao, China), LiChroprep RP-C18 gel (Merck, 40–63 μm, Darmstadt, Germany) and Sephadex LH-20 (Gytiva Sweden AB, Upsala, Sweden). Fractions were monitored by thin-layer chromatography (TLC), and spots were visualized by heating silica gel plates sprayed with 10% H_2SO_4/CH_3CH_2OH. A semipreparative HPLC was run on a Shimadzu system (Shimadzu Corporation, Nakagyo-

ku, Kyoto, Japan) with a Shim-pack Scepter C18-120 (4.6 mm × 250 mm, 5 μm). The 3T3-L1 mouse preadipocytes were purchased from the American Type Culture Collection (ATCC, Manassas, VA, USA). High-glucose DMEM, low-glucose DMEM, Pen-Strep solution (P/S), insulin, certified fetal bovine serum (FBS), special newborn calf serum (NBCS), and phosphate buffered saline (PBS) were purchased from Biological Industries (Shanghai, China). 3-Isobutyl-1-methylxanthine (IBMX) and dexamethasone (DEX) were obtained from Sigma-Aldrich (St. Louis, MO, USA). Rosiglitazone (ROSI) was purchased from Meilun Biotech Co., Ltd. (Dalian, Liaoning, China). Dimethyl sulfoxide (DMSO) was obtained from Solarbio (Beijing, China). The glucose test kit was purchased from Rongsheng Biotech Co., Ltd. (Shanghai, China). CellTiter 96® AQueous One Solution Cell Proliferation Assay was also acquired (Promega Corporation, Madison, WI, USA). α-Glucosidase (33 U/mg), acarbose, 4-nitrophenyl-α-D-glucopyranoside (*p*NPG), and ascorbic acid were purchased from Yuanye Biotech Co., Ltd. (Shanghai, China). The other chemicals and reagents were purchased from local suppliers. The absorbance was measured by a microplate reader (Molecular Devices, Palo Alto, Santa Clara, CA, USA).

3.2. Plant Materials

KF, the fruits of *Kochia scoparia* (Linn.) Schrad produced in Shandong, were purchased from Yunnan Lvsheng Pharmaceutical Co., Ltd (Yunnan, China). in 2019, and identified by Prof. Yumei Zhang of Xishuangbanna Tropical Botanical Garden, Chinese Academy of Sciences. A voucher specimen (No. 2019001) of KF was deposited in the Innovative Drug Research Group, Xishuangbanna Tropical Botanical Garden, Chinese Academy of Sciences.

3.3. Extraction and Isolation

The air-dried fruits of *K. scoparia* (20 kg) were extracted four times (7, 3, 3, 1 day, respectively) with 80% ethanol (45, 30, 30, 30 L, respectively) at room temperature. The extracts were filtered and evaporated under reduced pressure to obtain the ethanol extract of Kochiae Fructus (EE, 2.03 kg). Then, the EE (2.0 kg) was subjected to silica gel column chromatography and eluted with petroleum ether, ethyl acetate, and ethanol to obtain the petroleum ether fraction of EE (PEF, 0.15 kg), ethyl acetate fraction of EE (EAF, 0.26 kg), and ethanol fraction of EE (ETF, 1.40 kg), respectively. The ETF (1.40 kg) was subjected to silica gel column chromatography and eluted with ethyl acetate/methanol (3:1, 0:1) to yield two fractions (Fr. 1, Fr. 2). Then, the two fractions were dissolved with 20% (*v*/*v*) ethanol (EtOH)/water (H$_2$O) solution and centrifuged at 5000 rpm for fifteen minutes, respectively. Two supernatants were evaporated under reduced pressure to yield two sub-fractions (Fr. 1.1, Fr. 2.1), respectively. Removal of the supernatant gave the sediment (Fr. 3) by rotary evaporators. Fr. 1.1 (114.7 g) was chromatographed on a silica gel column (200–300 mesh) and eluted with chloroform (CHCl$_3$)/methanol (MeOH) gradient system (20:1 to 1:1) to yield two sub-fractions 1.1.1 and 1.1.2). Fr. 1.1.1 (74.6 g) was subjected to repeated column chromatography over silica gel, RP-C18, Sephadex LH-20, preparative HPLC, to afford compounds **3** (3.08 mg), **7** (4.21 mg), **8** (9.11 mg), and **12** (17.52 mg). Fr. 1.1.2 (42.4 g) was subjected to repeated column chromatography over silica gel, RP-C18, Sephadex LH-20 (Gytiva Sweden AB, Upsala, Sweden), preparative HPLC, to afford compounds **5** (3.04 mg), **13** (2.75 mg), **14** (16.5 mg), **15** (3.28 mg), **16** (2.05 mg), and **17** (5.37 mg). Fr. 2.1 (100 g) was separated by Sephadex LH-20 column using CHCl$_3$-MeOH isocratic system (1:1) to afford three sub-fractions (Fr. 2.1.1, Fr. 2.1.2, and Fr. 2.1.3). Fr. 2.1.1 (27.7 g) was subjected to repeated column chromatography over RP-C18 and a preparative HPLC to afford compounds **1** (5.03 mg), **2** (2.86 mg), **9** (3.28 mg) and **11** (2.46 mg). Fr. 3 (100 g) was ground and dissolved by heating with 100% ethanol solution at 60 °C, filtered, and the ethanol in the filtrate was removed under reduced pressure to obtain sub-fraction 3.1 (Fr. 3.1). Fr. 3.1 (86 g) was ground into powder and dissolved with ethanol (86 × 5 mL); the mixture solution was stirred using a magnetic stirrer at 600 rpm for 24 h. Finally, the filter residue was obtained by filtration. After repeating the above operation four times, the filter residue was finally obtained (Fr. 3.1.1, 30 g). Fr. 3.1.1 (30 g) was purified by

a preparative HPLC (MeOH-H$_2$O-acetic acid (CH$_3$COOH), 85:15:0.2, isocratic) to give compound **4** (5.2 g). The EAF (260 g) was subjected to silica gel column chromatography and eluted with CHCl$_3$/MeOH (50:1 to 0:1) to yield compound **6** (3.37 mg). The PEF (150 g) was subjected to silica gel column chromatography and eluted with petroleum ether/CHCl$_3$ (50:1 to 0:1) to yield compound **10** (56.1 g).

3.3.1. 3(β)-3-O-β-D-xylopyranosly(1→3)-β-D-glucopyranosiduronic acid 12-en-23,28-dioic acid (**1**)

The molecular formula was C$_{41}$H$_{62}$O$_{15}$, white amorphous powder; [α]25 D + 17.1° (c 0.187, MeOH); UV/Vis (MeOH, λ$_{max}$, nm) (log ε): 203 (3.92). IR (KBr) v_{max} 3434, 2928, 2870, 1625, 1385, 1038 cm^{-1}; ECD (MeOH, λ$_{max}$, nm) (△ε): 195 (8.22), 262 (0.28). ^{1}H NMR (500 MHz, methanol-d_4) and ^{13}C NMR (125 MHz, methanol-d_4), see Tables 1 and 2; HR-ESI-MS *m/z* 396.1971 [M-2H]$^{2-}$ (calcd 396.1972) (see Supplementary Data).

3.3.2. 3(β)-3-*O*-*β*-D-xylopyranosly(1→3)-*β*-D-glucopyranosiduronic acid 6-methyl ester-12-en-23,28-dioic acid (**2**)

The molecular formula was C$_{42}$H$_{64}$O$_{15}$, white amorphous powder; [α]25 D + 4.5° (c 0.089, MeOH); UV/Vis (MeOH, λ$_{max}$, nm) (log ε): 203 (3.92). IR (KBr) v_{max} 3419, 2927, 2864, 1694, 1386, 1258, 1037 cm^{-1}; ECD (MeOH, λ$_{max}$, nm) (△ε): 195 (4.62), 262 (0.23). ^{1}H NMR (500 MHz, methanol-d_4) and ^{13}C NMR (125 MHz, methanol-d_4), see Tables 1 and 2; HR-ESI-MS *m/z* 403.2053 [M-2H]$^{2-}$ (calcd 403.2050) (see Supplementary Data).

3.3.3. 2β,3β-dihydroxyolean-12-en-28-oic acid 28-*O*-*β*-D-glucopyranoside (**3**)

The molecular formula was C$_{36}$H$_{58}$O$_9$, white amorphous powder; [α]25 D + 22.67° (c 0.172, MeOH); UV/Vis (CH$_3$OH, λ$_{max}$, nm) (log ε): 203 (3.76). IR (KBr) v_{max} 3422, 2928, 2867, 1738, 1385, 1259, 1071, 1030 cm^{-1}; ECD (MeOH, λ$_{max}$, nm) (△ε): 195 (6.31), 241 (0.40). ^{1}H NMR (500 MHz, methanol-d_4) and ^{13}C NMR (125 MHz, methanol-d_4), see Tables 1 and 2; HR-ESI-MS *m/z* 657.3973 [M+Na]$^+$ (calcd 657.3973) (see Supplementary Data).

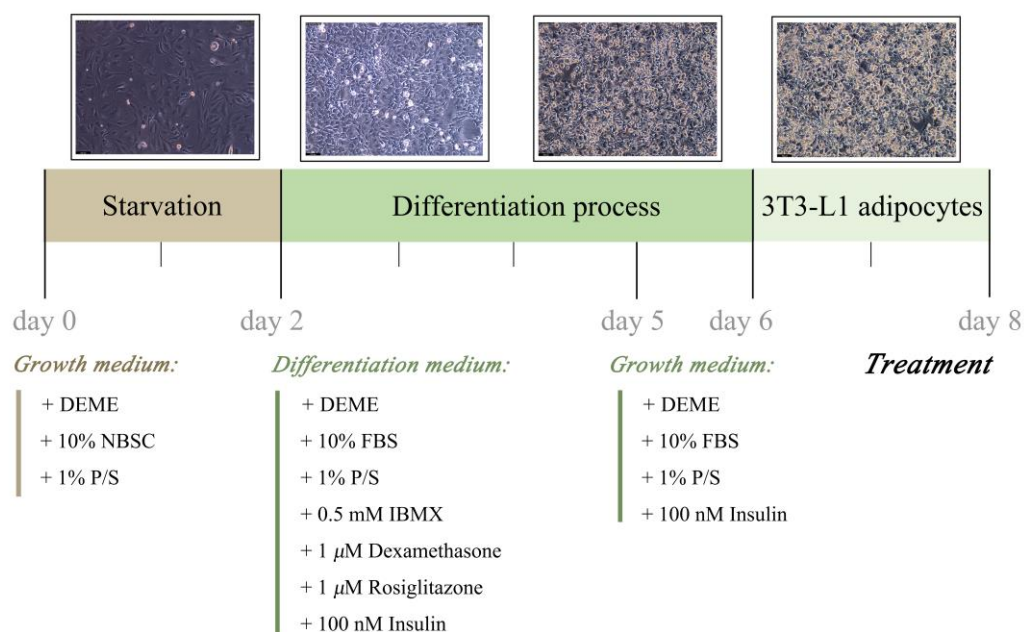### *3.4. 3T3-L1 Preadipocytes Culture and Differentiation*

The murine 3T3-L1 preadipocytes were supplied by the American Type Culture Collection (ATCC, Manassas, VA, USA). The cells were cultured in high-glucose DMEM supplemented with 10% (*v/v*) newborn calf serum (NBCS), 1% (*v/v*) Pen-Strep solution (P/S) at 37 °C in a humidified atmosphere of 5% CO$_2$, and then starved until the cells reached confluence (day 0). Two days later (day 2), the cells were cultured in DMEM supplemented with 10% (*v/v*) fetal bovine serum (FBS), 1% (*v/v*) P/S, 0.5 mM 3-isobutyl-1-methylxanthine (IBMX), 1 μM dexamethasone (DEX), 1 μM rosiglitazone (ROSI) and 100 nM insulin. Three days after (day 5) the induction, the culture medium was replaced with DMEM containing 10% (*v/v*) FBS, 1% (*v/v*) P/S, and 100 nM insulin for one day (day 6). Then the cells were completely differentiated into mature adipocytes (Figure 11).

3.5. Glucose Uptake and Cell Viability Assays

The mature adipocytes were inoculated in a 96-well plate at 5×10^4 cells per well for 24 h. The 3T3-L1 adipocytes were divided into model groups (blank control), insulin group (250 ng/mL, positive control), and sample group (20 μM). After 24 h of administration, 10 μL medium was used to measure the glucose content. The absorbance value was detected by a microplate reader at 505 nm. The glucose uptake rate was calculated as follows:

$$\text{Glucose uptake rate (\%)} = [1 - A_2/A_1] \times 100 \qquad (1)$$

where A$_1$ is the absorbance of the mixed-glucose, DMEM-supplemented control, and A$_2$ is the absorbance of the blank, insulin, or sample group.

Figure 11. Differentiation process schedule. DMEM, dulbecco's modified eagle medium; NBCS, special newborn calf serum; P/S, penicillin/streptomycin; FBS, certified fetal bovine serum; IBMX, 3-isobutyl-1-methyl-xanthine.

Cell viability was detected by using a CellTiter 96® AQueous One Solution Cell Proliferation Assay (Promega Corporation, Madison, WI, USA) according to the manufacturer's instructions after the glucose uptake experiment [50]. CellTiter 96® AQueous One Solution Cell Proliferation Assay reagent (20 μL/well) was added to the plate and incubated at 37 °C for 180 min before absorbance was measured at 490 nm, and the relative cell viability was calculated as follows:

$$\text{Relative cell viability (\%)} = A_1/A_2 \times 100 \tag{2}$$

where A_1 is the absorbance of the blank control, and A_2 is the absorbance of the sample group.

3.6. In Vitro α-Glucosidase Inhibition Assay

The α-glucosidase inhibition assay was carried out on the basis of the method reported by Zhang et al., with minor modifications [51]. Briefly, α-glucosidase (0.1 U/mL), *p*NPG (5 mM) and Na_2CO_3 (0.5 M) were prepared in PBS (0.1 M, pH 6.8), and the samples were diluted to different concentrations (0.0625, 0.125, 0.25, 0.5, 1, and 2 mM) using PBS. In a 96-well microplate, a mixture of 80 μL PBS, 10 μL sample, and 50 μL α-glucosidase solution were added and incubated for 15 min at 37 °C, 10 μL PBS used as a blank control. To initiate the reaction, *p*NPG (40 μL) was added to the reaction mixture and incubated at 37 °C for 30 min. The reaction was terminated by adding 20 μL of Na_2CO_3, after which the absorbance was determined at 405 nm by a microplate reader (SpectraMax190, Micro-g Biotech, Guangzhou, China). Acarbose was used as a positive control in this α-glucosidase inhibition assay. IC_{50} values were defined as the concentration of the compound required to inhibit 50% of α-glucosidase activity under assay conditions. The α-glucosidase inhibition activity was calculated as follows:

$$\text{Inhibition rate (\%)} = (A_1 - A_2)/A_1 \times 100 \tag{3}$$

where A_1 is the OD value of the blank control, A_2 is the OD value of the tested samples, and the analysis was performed in triplicates.

3.7. Kinetics Involved in the Inhibition of α-Glucosidase

The kinetic analysis of compounds **3**, **9**, and **13** were measured using the reaction conditions in Section 3.6. Typically, three different concentrations of each compound around the IC$_{50}$ values were chosen. Under each concentration, α-glucosidase activity was assayed by varying the concentration of *p*NPG as a substrate [46]. The inhibition types of active compounds were determined by Lineweaver–Burk plots [the inverse of velocity ($1/v$) against the inverse of the substrate concentration ($1/[p$NPG])] with substrate concentrations of 1.25, 2.5, 5, 10, 20 μM. K_i and K_i' values were determined from $1/v$ versus [I] (Dixon plot) and S/v versus [I] plots, respectively.

3.8. Molecular Docking

The molecular docking approach can be used to model the interaction between a small molecule and a protein at the atomic level [52]. The structure of α-glucosidase (PDB ID: 3A4A) was obtained from the Online Protein Data Bank [53], and the 3D structures of the ligands were generated by Chem3D Pro (version: 14.0). Complexed ligands and water molecules in the crystal structure of α-glucosidase were virtually removed by PyMOL Win application (PyMOL, version: 2.4.0). Gasteiger charges and essential hydrogen atoms were added by using the AutoDock tools (ADT, version: 1.5.6). The cubic grid box dimensions of α-glucosidase were defined as x = 98, y = 126, and z = 102 Å with spacing of 0.692 Å. Finally, the PyMOL molecular graphics system (version 2.4.0) was used to visualize ligand–enzyme interactions.

3.9. Statistical Analysis

IBM SPSS Statistics for Windows, version 26.0 (IBM Corp., Armonk, NY, USA), was used to analyze all of the data. The experiments were carried out in triplicates and the results were expressed as an average of the three measurements $\pm$ SD. One-way analysis of variance (ANOVA) was used to compare the means of different analysis investigations. Differences were considered significant when * $p < 0.05$, ** $p < 0.01$, *** $p < 0.001$.

4. Conclusions

Seventeen compounds, including three previously undescribed and fourteen known triterpenes, were isolated from the ethanol extract of KF. We detected their hypoglycemic activities via assays for α-glucosidase inhibition and glucose uptake of 3T3-L1 adipocytes. Next, we performed enzyme kinetics and molecular docking investigations to analyze the possible mechanisms against enzymes. The results of the glucose uptake experiment showed compound **13** had a significant promotion on glucose uptake rate of 3T3-L1 adipocytes ($p < 0.001$). Simultaneously, enzyme-inhibition results suggested that compounds **3**, **9**, and **13** possessed potent inhibitory effects on α-glucosidase, and their enzymatic kinetics on α-glucosidase showed that they are mixed-type inhibitors. The hydroxyl group in the ring of the pentacyclic triterpene played a key role in maintaining α-glucosidase inhibitory activity according to the docking simulation. In summary, this study enriched the chemical composition diversity of KF and provided effective evidence for its use in hypoglycemic herbal medicine.

References

1. Peng, D.; Tian, W.N.; An, M.Q.; Chen, Y.L.; Zeng, W.S.; Zhu, S.Y.; Li, P.; Du, B. Characterization of antidiabetic effects of *Dendrobium officinale* derivatives in a mouse model of type 2 diabetes mellitus. *Food Chem.* **2023**, *399*, 133974. [CrossRef]
2. Sun, H.; Saeedi, P.; Karuranga, S.; Pinkepank, M.; Ogurtsova, K.; Duncan, B.B.; Stein, C.; Basit, A.; Chan, J.C.N.; Mbanya, J.C.; et al. IDF Diabetes Atlas: Global, regional and country-level diabetes prevalence estimates for 2021 and projections for 2045. *Diabetes Res. Clin. Pract.* **2022**, *183*, 109–119. [CrossRef] [PubMed]
3. Tello, J.D.C.; Moretta, D.E.S.; HernÁndez, G.J.V.; Medina, L.S.H. Type 2 diabetes mellitus and management of isolated hyperglycemia: A review. *Innovare J. Health Sci.* **2022**, *10*, 1–4. [CrossRef]
4. Solis-Herrera, C.; Triplitt, C.; Cersosimo, E.; DeFronzo, R.A. *Site of Insulin Resistance in Type 2 Diabetes. Pathogenesis of Type 2 Diabetes Mellitus*, 3rd ed.; Feingold, K.R., Anawalt, B., Boyce, A., Chrousos, G., de Herder, W.W., Dhatariya, K., Dungan, K., Hershman, J.M., Hofland, J., Kalra, S., et al., Eds.; Endotext [Internet]: South Dartmouth, MA, USA, 2021.
5. Tomasik, P.; Horton, D. Enzymatic conversions of starch. *Adv. Carbohydr. Chem. Biochem.* **2012**, *68*, 59–436. [CrossRef] [PubMed]
6. Lim, S.H.; Yu, J.S.; Lee, H.S.; Choi, C.I.; Kim, K.H. Antidiabetic flavonoids from fruits of *Morus alba* promoting insulin-stimulated glucose uptake via Akt and AMP-activated protein kinase activation in 3T3-L1 adipocytes. *Pharmaceutics* **2021**, *13*, 526. [CrossRef] [PubMed]
7. Liu, S.K.; Hao, H.; Bian, Y.; Ge, Y.X.; Lu, S.; Xie, H.X.; Wang, K.M.; Tao, H.; Yuan, C.; Zhang, J.; et al. Discovery of new α-glucosidase inhibitors: Structure-based virtual screening and biological evaluation. *Front. Chem.* **2021**, *9*, 639279. [CrossRef] [PubMed]
8. Vishwanath, D.; Srinivasan, H.; Patil, M.S.; Seetarama, S.; Agrawal, S.K.; Dixit, M.N.; Dhar, K. Novel method to differentiate 3T3-L1 cells in vitro to produce highly sensitive adipocytes for a GLUT4 mediated glucose uptake using fluorescent glucose analog. *J. Cell. Commun. Signal.* **2013**, *7*, 129–140. [CrossRef] [PubMed]
9. Kim, S.H.; Shin, E.J.; Kim, E.D.; Bayaraa, T.; Frost, S.C.; Hyun, C.K. Berberine activates GLUT1-mediated glucose uptake in 3T3-L1 adipocytes. *Biol. Pharm. Bull.* **2007**, *30*, 2120–2125. [CrossRef] [PubMed]
10. Shyni, G.L.; Kavitha, S.; Indu, S.; Arya, A.D.; Anusree, S.S.; Vineetha, V.P.; Vandana, S.; Sundaresan, A.; Raghu, K.G. Chebulagic acid from *Terminalia chebula* enhances insulin mediated glucose uptake in 3T3-L1 adipocytes via PPARγ signaling pathway. *Biofactors* **2014**, *40*, 646–657. [CrossRef] [PubMed]
11. Park, H.; Hwang, K.Y.; Oh, K.H.; Kim, Y.H.; Lee, J.Y.; Kim, K. Discovery of novel α-glucosidase inhibitors based on the virtual screening with the homology-modeled protein structure. *Bioorg. Med. Chem.* **2008**, *16*, 284–292. [CrossRef]
12. Kim, J.H.; Kim, H.Y.; Jin, C.H. Mechanistic investigation of anthocyanidin derivatives as α-glucosidase inhibitors. *Bioorg. Chem.* **2019**, *87*, 803–809. [CrossRef]
13. Li, D.Q.; Qian, Z.M.; Li, S.P. Inhibition of three selected beverage extracts on α-glucosidase and rapid identification of their active compounds using HPLC-DAD-MS/MS and biochemical detection. *J. Agric. Food Chem.* **2010**, *58*, 6608–6613. [CrossRef] [PubMed]
14. Yoshikawa, M.; Dai, Y.; Shimada, H.; Morikawa, T.; Matsumura, N.; Yoshizumi, S.; Matsuda, H.; Matsuda, H.; Kubo, M. Studies on Kochiae Fructus. II. On the saponin constituents from the fruit of chinese *Kochia scoparia* (Chenopodiaceae): Chemical structures of kochianosides I, II, III, and IV. *Chem. Pharm. Bull.* **1997**, *45*, 1052–1055. [CrossRef]
15. Matsuda, H.; Li, Y.; Murakami, T.; Matsumura, N.; Yamahara, J.; Yoshikawa, M. Antidiabetic principles of natural medicines. III. Structure-related inhibitory activity and action mode of oleanolic acid glycosides on hypoglycemic activity. *Chem. Pharm. Bull.* **1998**, *46*, 1399–1403. [CrossRef] [PubMed]
16. Xu, Y.H.; Huang, H.; Zhang, N.; Kong, D.Y.; Hua, M.L. Studies on the flavone glycosides from Fructus Kochiae. *J. Asian Nat. Prod. Res.* **2014**, *16*, 141–147. [CrossRef] [PubMed]
17. Lu, X.H.; Xu, X.D.; Fu, H.W.; Chen, B.; Tian, J.K.; Zhang, L. Study on chemical constituents of *Kochia scoparia*. *Chin. Pharm. J.* **2012**, *47*, 338–342.
18. Houlihan, A.J.; Conlin, P.; Chee-Sanford, J.C. Water-soluble exudates from seeds of *Kochia scoparia* exhibit antifungal activity against *Colletotrichum graminicola*. *PLoS ONE* **2019**, *14*, e0218104. [CrossRef] [PubMed]
19. Yang, M.; Li, Q.; Cai, J.; Yang, S.B. Supercritical CO_2 extraction and GC-MS analysis of Kochia Fructus oil. *Zhong Yao Cai* **2003**, *7*, 494. [CrossRef]
20. Zou, W.; Tang, Z.; Long, Y.; Xiao, Z.Q.; Ouyang, B.; Liu, M.H. Kochiae Fructus, the fruit of common Potherb *Kochia scoparia* (L.) Schrad: A review on phytochemistry, pharmacology, toxicology, quality control, and pharmacokinetics. *Evid. Based Complement. Alternat. Med.* **2021**, *2021*, 5382684. [CrossRef] [PubMed]

21. National Pharmacopoeia Commission. *The Pharmacopoeia of the People's Republic of China*, 1st ed.; China Medical Science and Technology Press: Beijing, China, 2020.
22. Jo, S.; Ryu, J.; Han, H.Y.; Lee, G.; Ryu, M.H.; Kim, H. Anti-inflammatory activity of *Kochia scoparia* fruit on contact dermatitis in mice. *Mol. Med. Rep.* **2016**, *13*, 1695–1700. [CrossRef] [PubMed]
23. Dai, Y.; Xia, Y.F.; Lin, S.L. Studies on the hypoglycemic mechanism of n-butanol fraction from Fructus Kochiae. *Pharmacol. Clin. Chin. Mater. Med.* **2003**, *19*, 21–24.
24. Yan, M.R.; Zhang, W.B.; Luo, G.P.; Wang, X.N.; Feng, S.M.; Zhao, N. Screening chemical constituents with antioxidative activity from the Kochiae Fructus. *Chin. Med. J. Res. Pract.* **2019**, *33*, 29–32.
25. Wang, J.; Han, Y.; Wang, M.; Zhao, Q.Q.; Chen, X.F.; Liu, X.B. Natural triterpenoid saponin momordin Ic suppresses HepG2 cell invasion via COX-2 inhibition and PPARγ activation. *Toxicol. In Vitro* **2020**, *65*, 104784. [CrossRef] [PubMed]
26. Wang, J.N.; Liu, Q.Y.; Yao, C.H.; Chen, S.J.; Song, L.Y.; Guan, P.; Shao, L.J.; She, Y.Y.; Chi, H.Y. Normative research on bacteriostasis and relieving itching external therapeutic function of Kochiae Fructus. *Zhong Yao Cai* **2012**, *35*, 1974–1977. [CrossRef]
27. Kubo, M.; Matsuda, H.; Dai, Y.; Ido, Y.; Yoshikawa, M. Studies on Kochiae Fructus. I. Antipruritogenic effect of 70% ethanol extract from kochiae fructus and its active component. *Yakugaku Zasshi* **1997**, *117*, 193–201. [CrossRef] [PubMed]
28. Matsuda, H.; Dai, Y.; Ido, Y.; Yoshikawa, M.; Kubo, M. Studies on Kochiae Fructus. IV. Anti-allergic effects of 70% ethanol extract and its component, momordin Ic from dried fruits of *Kochia scoparia* L. Biol. Pharm. Bull. **1997**, *20*, 1165–1170. [CrossRef] [PubMed]
29. Dai, Y.; Xia, Y.F.; Chen, H.B.; Matsuda, H.; Kubo, M. Inhibition of immediate and delayed type hypersensitivity by the 70% ethanolic extract from *Fructus kochiae*. *Chin. J. Mod. Appl. Pharm.* **2001**, *1*, 8–9. [CrossRef]
30. Kim, N.Y.; Lee, M.K.; Park, M.J.; Kim, S.J.; Park, H.J.; Choi, J.; Kim, S.H.; Cho, S.Y.; Lee, J. Momordin Ic and oleanolic acid from Kochiae Fructus reduce carbon tetrachloride-induced hepatotoxicity in rats. *J. Med. Food* **2005**, *8*, 177–183. [CrossRef] [PubMed]
31. Matsuda, H.; Dai, Y.; Ido, Y.; Murakami, T.; Matsuda, H.; Yoshikawa, M.; Kubo, M. Studies on Kochiae Fructus. V. Antipruritic effects of oleanolic acid glycosides and the structure-requirement. *Biol. Pharm. Bull.* **1998**, *21*, 1231–1233. [CrossRef] [PubMed]
32. Amimoto, K.; Yoshikawa, K.; Arihara, S. Triterpenoid saponins of Aquifoliaceous plants. VIII. Ilexosides XXIX-XXXII from the leaves of *Ilex rotunda* THUNB. *Chem. Pharm. Bull.* **1992**, *40*, 3138–3141. [CrossRef]
33. Wen, Y.; Chen, Y.; Cui, Z.; Li, J.; Wang, Z. Triterpenoid glycosides from the fruits of *Kochia scoparia*. *Planta Med.* **1995**, *61*, 450–452. [CrossRef] [PubMed]
34. Han, L.K.; Nose, R.; Li, W.; Gong, X.J.; Zheng, Y.N.; Yoshikawa, M.; Koike, K.; Nikaido, T.; Okuda, H.; Kimura, Y. Reduction of fat storage in mice fed a high-fat diet long term by treatment with saponins prepared from *Kochia scoparia* fruit. *Phytother. Res.* **2006**, *20*, 877–882. [CrossRef] [PubMed]
35. Kawamura, N.; Watanabe, H.; Oshio, H. Saponins from roots of *Momordica cochinchinensis*. *Phytochemistry* **1988**, *27*, 3585–3591. [CrossRef]
36. Hossain, M.A.; Ismail, Z. Isolation and characterization of triterpenes from the leaves of *Orthosiphon stamineus*. *Arab. J. Chem.* **2013**, *6*, 295–298. [CrossRef]
37. Xie, L.X.; Zhang, H.C.; Wang, H.Y.; Wang, Y.; Wang, F.L.; Sun, J.Y. Two new triterpenoids from *Gypsophila oldhamiana*. *Nat. Prod. Res.* **2016**, *30*, 1068–1074. [CrossRef] [PubMed]
38. Suthar, S.K.; Hooda, A.; Sharma, A.; Bansal, S.; Monga, J.; Chauhan, M.; Sharma, M. Isolation optimisation, synthesis, molecular docking and in silico ADMET studies of lantadene a and its derivatives. *Nat. Prod. Res.* **2021**, *35*, 3939–3944. [CrossRef] [PubMed]
39. Xue, J.; Xie, L.; Liu, B.R.; Yu, L.X. Triterpenoids from the fruits of *Forsythia suspensa*. *Chin. J. Nat. Med.* **2010**, *8*, 414–418. [CrossRef]
40. Liu, L.; Li, H.B.; Hu, K.W.; Xu, Q.L.; Wen, X.A.; Cheng, K.G.; Chen, C.P.; Yuan, H.L.; Dai, L.; Sun, H.B. Synthesis and anti-inflammatory activity of saponin derivatives of δ-oleanolic acid. *Eur. J. Med. Chem.* **2021**, *209*, 112932. [CrossRef] [PubMed]
41. Borel, C.; Gupta, M.P.; Hostettmann, K. Molluscicidal saponins from *Swartzia simplex*. *Phytochemistry* **1987**, *26*, 2685–2689. [CrossRef]
42. Kuroda, M.; Aoshima, T.; Haraguchi, M.; Young, M.C.M.; Sakagami, H.; Mimaki, Y. New oleanane glycosides from the roots of *Gomphrena macrocephala*. *Nat. Prod. Commun.* **2006**, *1*, 431–439. [CrossRef]
43. Lahrita, L.; Kato, E.; Kawabata, J. Uncovering potential of indonesian medicinal plants on glucose uptake enhancement and lipid suppression in 3T3-L1 adipocytes. *J. Ethnopharmacol.* **2015**, *168*, 229–236. [CrossRef] [PubMed]
44. Kalra, S. Alpha glucosidase inhibitors. *J. Pak. Med. Assoc.* **2014**, *64*, 474–476. [PubMed]
45. Huang, L.R.; Luo, H.; Li, Q.J.; Wang, D.P.; Zhang, J.X.; Hao, X.J.; Yang, X.S. Pentacyclic triterpene derivatives possessing polyhydroxyl ring A inhibit gram-positive bacteria growth by regulating metabolism and virulence genes expression. *Eur. J. Med. Chem.* **2015**, *95*, 64–75. [CrossRef] [PubMed]
46. Liu, Y.; Ma, L.; Chen, W.H.; Park, H.; Ke, Z.F.; Wang, B. Binding mechanism and synergetic effects of xanthone derivatives as noncompetitive α-glucosidase inhibitors: A theoretical and experimental study. *J. Phys. Chem. B* **2013**, *117*, 13464–13471. [CrossRef] [PubMed]
47. Zeng, L.; Zhang, G.W.; Liao, Y.J.; Gong, D.M. Inhibitory mechanism of morin on α-glucosidase and its anti-glycation properties. *Food Funct.* **2016**, *7*, 3953–3963. [CrossRef] [PubMed]
48. Sengupta, S.; Mukherjee, A.; Goswami, R.; Basu, S. Hypoglycemic activity of the antioxidant saponarin, characterized as α-glucosidase inhibitor present in *Tinospora cordifolia*. *J. Enzyme Inhib. Med. Chem.* **2009**, *24*, 684–690. [CrossRef] [PubMed]
49. Morris, G.M.; Lim-Wilby, M. Molecular docking. *Methods Mol. Biol.* **2008**, *443*, 365–382. [CrossRef] [PubMed]

50. Akter, S.; Addepalli, R.; Netzel, M.E.; Tinggi, U.; Fletcher, M.T.; Sultanbawa, Y.; Osborne, S.A. Antioxidant-rich extracts of *Terminalia ferdinandiana* interfere with estimation of cell viability. *Antioxidants* **2019**, *8*, 1–8. [CrossRef] [PubMed]

51. Zhang, K.; Chen, X.L.; Zhao, X.; Ni, J.Y.; Wang, H.L.; Han, M.; Zhang, Y.M. Antidiabetic potential of Catechu via assays for α-glucosidase, α-amylase, and glucose uptake in adipocytes. *J. Ethnopharmacol.* **2022**, *291*, 115–118. [CrossRef] [PubMed]

52. Meng, X.Y.; Zhang, H.X.; Mezei, M.; Cui, M. Molecular docking: A powerful approach for structure-based drug discovery. *Curr. Comput. Aided Drug Des.* **2011**, *7*, 146–157. [CrossRef] [PubMed]

53. Yamamoto, K.; Miyake, H.; Kusunoki, M.; Osaki, S. Crystal structures of isomaltase from *Saccharomyces cerevisiae* and in complex with its competitive inhibitor maltose. *FEBS J.* **2010**, *277*, 4205–4214. [CrossRef] [PubMed]